Comparative study of electroreduction of iron oxide using acidic and alkaline electrolytes for sustainable iron production

Electrochimica Acta 467 (2023) 142942

Contents lists available at ScienceDirect

Electrochimica Acta

journal homepage: www.journals.elsevier.com/electrochimica-acta

Comparative study of electroreduction of iron oxide using acidic and alkaline electrolytes for sustainable iron production

Akmal Irfan Majid [a,d], Niels van Graefschepe [a], Giulia Finotello [a,c,*], John van der Schaaf [b,c], Niels G. Deen [a,c], Yali Tang [a,c]

[a] Power and Flow Section, Department of Mechanical Engineering, Eindhoven University of Technology, PO Box 513, 5600 MB, Eindhoven, The Netherlands
[b] Sustainable Process Engineering, Department of Chemical Engineering and Chemistry, Eindhoven University of Technology, PO Box 513, 5600 MB, Eindhoven, The Netherlands
[c] Eindhoven Institute for Renewable Energy Systems (EIRES), Eindhoven University of Technology, PO Box 513, 5600 MB, Eindhoven, The Netherlands
[d] Department of Mechanical and Industrial Engineering, Faculty of Engineering, Universitas Gadjah Mada, Jl. Grafika No. 2 Kampus UGM, 55281, Yogyakarta, Indonesia

ARTICLE INFO

Keywords:
Iron oxide reduction
Electrodeposition
Dendrites
Sustainable ironmaking
Metal fuels

ABSTRACT

Sustainable iron production is largely driven by the urgency to reduce the extensive energy consumption and emissions in the iron/steel sectors. Low-temperature electroreduction of iron oxide technology is thus revived since it directly utilizes (green) electrical energy with a competitive energy consumption compared to the thermochemical reduction approach. In the present work, we perform theoretical and experimental studies for comparison of electroreduction of iron oxide in aqueous alkaline and acidic electrolytes. Electrochemical reduction and deposition behavior are experimentally investigated using a lab-scale cell containing an electrolyte suspended with micron-sized Fe_2O_3 (hematite) powders. The effects of current density and hematite mass fraction on current efficiency are evaluated, as well as the total energy consumption. Results of chronopotentiometry and cyclic voltammograms (CV) reveal the electrochemical properties of each system. The CV's cathodic peaks, corresponding to the reduction of iron oxides to iron, are observed only in the alkaline system where the iron oxide can be reduced at about −1.4 V (vs. Ag/AgCl). It is also found that the alkaline system has higher current efficiency (25–30% higher) and lower energy consumption (~30% lower) than the acidic system. The cleaning of the deposit is also easier for the alkaline system, resulting in an iron product of high purity. Concerning the electrochemical performances and practicality, the alkaline electroreduction system shows promising potential for sustainable iron production.

1. Introduction

Energy transition and climate change trigger iron and steelmaking industries to take extensive actions toward sustainability where the reduction of greenhouse gas emissions and outspread utilization of renewable energy sources become the spotlight. The iron and steel industries are the world's second-largest consumer of coal after power plants [20,25]. Iron/steel production has been rising over the years and demand is projected to rise as well [40,47]. To date, coal and coke are mainly used in iron oxide conversion inside blast furnaces, known as the carbothermic process. Since this method still uses a lot of fossil fuels and emits significant amounts of carbon dioxide and undesirable residues, cleaner technology alternatives are unavoidably needed.

Over the last decades, several technological initiatives were started to suppress carbon emissions and develop more sustainable iron/steel production processes, particularly on the conversion of iron ore (which is primarily composed of hematite-Fe_2O_3) into metallic iron. Breakthrough technologies have been widely implemented in many countries [42,49] and are mainly based on: (i) the development of cleaner reduction agents (e.g., hydrogen), (ii) safe and environmentally friendly methods for the disposal of the blast furnace by-product, (iii) future encouragement of novel non-blast furnace technologies.

One of the developments that become increasingly attractive is the *"power-to-iron"* process [8], whereby the (renewable) oxide power is intensively utilized to produce valuable iron products via an electrolysis process at both high and low temperatures. For the high-temperature

* Corresponding author at: Department of Mechanical Engineering, Eindhoven University of Technology, PO Box 513, Eindhoven, 5600 MB, The Netherlands.
E-mail address: g.finotello@tue.nl (G. Finotello).

https://doi.org/10.1016/j.electacta.2023.142942
Received 16 May 2023; Received in revised form 15 July 2023; Accepted 24 July 2023
Available online 26 July 2023

approach, the so-called molten oxide electrolysis (MOE), direct iron production is realized at a molten metal state by dissolving iron oxide. Wiencke et al. [46] demonstrated that this technique produces liquid iron after magnetite decomposition at operating temperatures above 1538 °C. However, high operating temperatures require high energy input, leading to more complex cell designs [7]. Alternatively, the electrochemical reduction (electroreduction) of iron oxide can be conducted in aqueous electrolytes at relatively low temperatures (around 110 °C or lower). This low temperature electroreduction approach represents advantages in energy cost and simplicity of the system design and process chain.

Electroreduction of iron oxide is possible under both aqueous acidic and alkaline electrolytes [41], as shown in the Pourbaix diagram (Fig. 1). This diagram shows the thermodynamics stability of each species under different pH and potential conditions. Meanwhile, the low solubility of iron oxide in both solvents may become a particular challenge to perform a quick transformation for getting Fe-ions which can facilitate the electrodeposition. Ishikawa et al. [21] stated that increasing the temperature and concentration of alkali-hydroxide leads to higher hematite solubility. Moreover, the solubility of hematite in NaOH is higher than other alkali hydroxides such as potassium hydroxide (KOH) and lithium hydroxide (LiOH). Similarly, the low solubility of hematite in acidic media was also addressed by Lu and Muir [33] and Vehmaanperä et al. [45], just to name a few. Besides, hematite is also known as an electrically insulating material [11,36] that may contribute to ohmic drop. However, with an activation process, such as establishing an interface with an electrical conductor and simultaneously with an electrolyte, the insulating Fe_2O_3 can be reduced [34].

Among the reported studies in the open literature, the majority use alkaline-based electrolytes. Early studies have shown proofs-of-concept that iron oxide can be reduced in alkaline media, for example, sodium hydroxide [30] and potassium hydroxide [18]. Since then, successful iron oxide electroreduction in alkaline systems has been reported using various species of iron oxide (α-Fe_2O_3, Fe_3O_4, and α-FeOOH) with different chemical reactivity responses [16] and different compounds, such as red-mud of bauxite residue [1], hematite-based ceramics [31] and magnesium ferro spinel [32], as well as residual material from zinc and nickel production [19]. It is suggested that the full reduction process is achieved via several intermediate steps including hydroxide formation, for processes both with *suspension* [2,16,44,48] and *bulk iron oxide-based cathode* [3,4,22,35,50]. The most recent development/breakthrough in this low-temperature alkaline-based electrolysis of iron oxide is achieved by the Siderwin project [27], where a pilot plant with a technology readiness level (TRL) of 6 has been built and operated successfully. On the other hand, prior studies have also demonstrated successful electrodeposition of iron at low temperatures in acidic environments, for instance, sulfate system [15,37] and chlorine system [12,39]. Acidic bath solutions containing iron/ferrous salt, such as ferrous chloride ($FeCl_2$) and ferrous sulfate ($FeSO_4$) were used in those cases. Electrolytes containing suspensions of iron oxides as utilized in alkaline systems (e.g., in the Siderwin project) have not been tested in acidic systems, to the authors' best knowledge.

After a dedicated literature review, the authors identify that a detailed comparison of electrochemical and reduction performances, as well as the deposit morphology for low-temperature electrolysis of iron oxides between acidic and alkaline systems is missing. This knowledge gap might hinder the development of this technology in new applications. This is indeed the case in the context of recyclable iron fuel [9,13,24], where the iron powder is combusted and regenerated cyclically as dense CO_2-free energy carriers. For the regeneration of iron powder from combusted powder ("(Fe_2o_3) *powder to* (Fe) *powder*"), low temperature electroreduction offers an alternative to the thermochemical route in which high energy consumption and powder sintering seem to be big issues. For this new application development, the selection of electrolytes is crucial. Despite higher faraday efficiency reported for alkaline systems, brittle iron deposits often found in acidic baths might offer an opportunity for easier harvest of the deposited iron in the form of powder.

Under this background, the current work aims to evaluate and compare the acidic and alkaline system features for low temperature electroreduction of iron oxide suspensions (*powder* to *powder*). This paper is organized as follows: the experimental details are explained in Section 2, where the electrolyte selection and preparation methods are also discussed. Subsequently, the experimental results of electrodeposition behavior and efficiency are elaborated in Section 3, and the main conclusions are presented in Section 4.

2. Experiments

2.1. Experimental apparatus

Fig. 2a presents the experimental setup which consists of a single

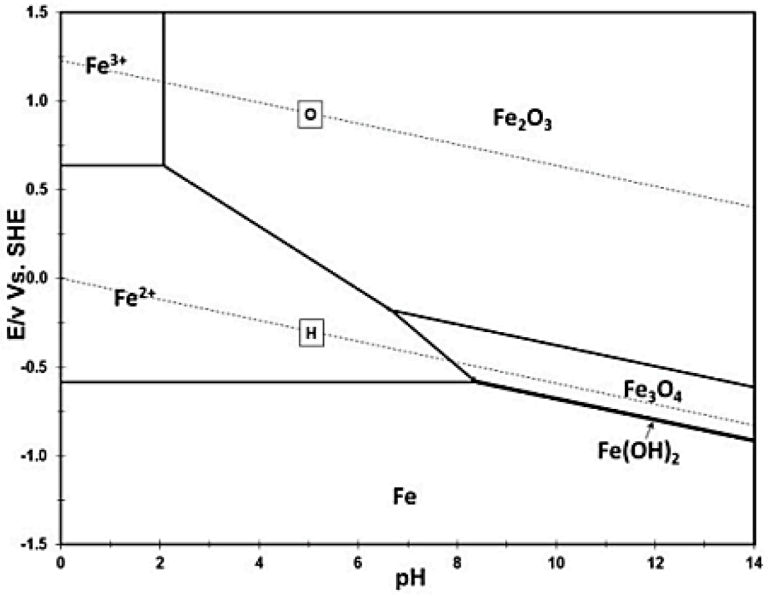

Fig. 1. Pourbaix diagram for iron-H_2O system in 25 °C, 1 bar (taken from Ning et al. [38]).

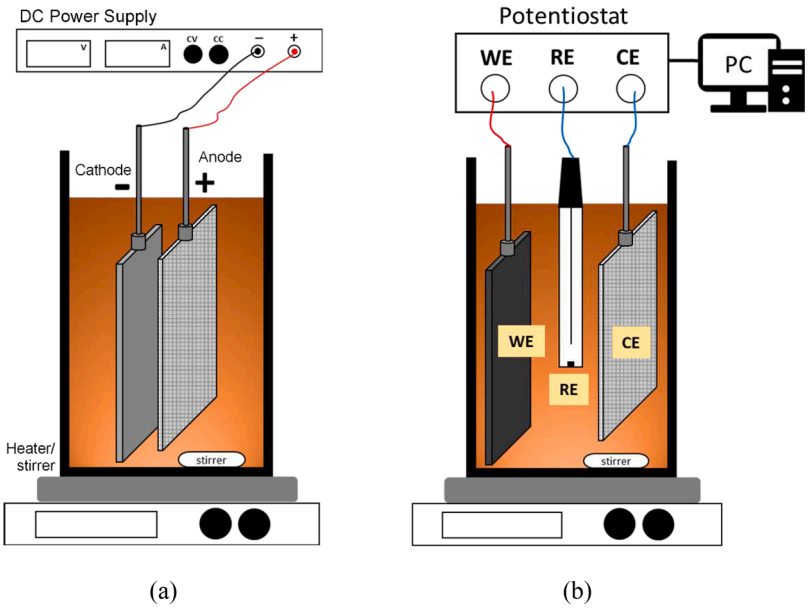

Fig. 2. Schematic overview of the experimental setup (a) Parallel plate setup for electroreduction. (b) 3-electrodes setup which uses a graphite working electrode (WE), a reference electrode (RE), and a counter electrode (CE). All electrodes are connected to a potentiostat and a personal computer (PC).

parallel plate electrolysis cell. The cell includes a 90 ml Pyrex beaker glass which is placed on a magnetic-heating plate (IKA RCT; equipped with an external thermocouple) to heat and agitate the electrolyte. The working electrode (cathode) is a stainless-steel plate (RVS-316 L) with a size of 15 mm x 40 mm x 2 mm. A thin rectangular platinum gauze/mesh electrode (0.12 mm aperture; wire diameter: 0.04 mm; 99.9 wt% purity) with a 25 mm x 50 mm surface area is used as a counter electrode (anode). The electrodes are maintained at a fixed distance of 20 mm by using stainless steel electrode holders. The power is supplied by a direct current (DC) power supply (Delta Elektronika; current range: 0–10 A, potential range: 0–30 V). The experiments are performed in batch mode with a constant low stirring rate of 100 rpm. For the cyclic voltammetry, a three-electrode setup (Fig. 2b) is used with the following configuration:

- Working electrode (WE): a graphite plate (15 mm x 40 mm x 2 mm).
- Counter electrode (CE): same as in the single parallel plate cell.
- Reference electrode (RE): an Ag/AgCl (3 M KCl) reference electrode.

These electrodes are connected to an Autolab potentiostat (PGSTAT30, current range: 0–1 A, potential range: 0–10 V) which is connected to a computer with Metrohm software to control and run the electroanalytical experiments.

2.2. Materials and chemicals

In this study, hematite (Fe_2O_3) powder (anhydrous, purity $\geq$ 96%, Sigma-Aldrich®) is used. The powder has a reddish-brown color as shown in Fig. 3a and a uniform morphology consisting of small crystals (<1 μm) as can be seen from Scanning Electron Microscope (SEM) images in Fig. 3b. The size distribution of the particles determined using laser diffraction (3P Bettersizer S3 Plus) is shown in Fig. 4. Most of the particles are smaller than 5 μm. The properties of acidic and alkaline electrolytes used in the iron electroreduction experiments are listed in Table 1. The choices of substance and concentration are based on studies reported by Allanore et al. [5] and Csicsovszki et al. [12].

2.3. Experimental procedure

2.3.1. Preparation of alkaline and acidic media

The aqueous alkaline solution is first heated to a temperature of 110 °C and then the Fe_2O_3 powder is gradually added. The alkaline

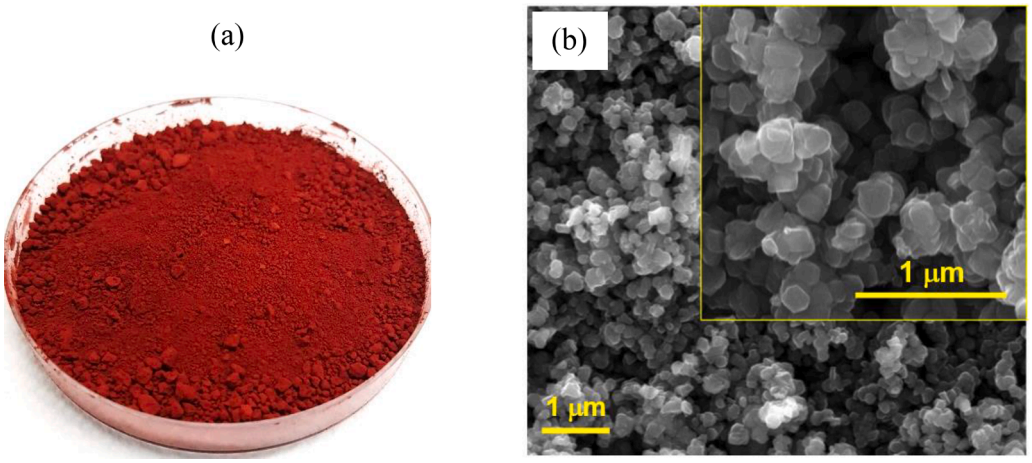

Fig. 3. Characteristics of hematite (Fe_2O_3) powder used in the present work. (a) The visual image of the powder (b) SEM image showing the morphology.

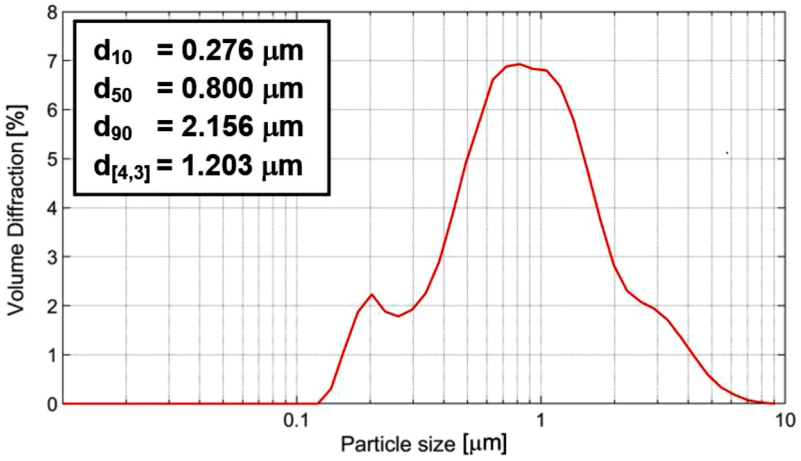

Fig. 4. Volume-based particle size distribution of hematite powder used in the present work.

Table 1
Properties of electrolytes used in this work.

Parameter	Aqueous acidic	Aqueous alkaline
Substance	Hydrochloric acid (HCl)	Sodium hydroxide (NaOH)
Mixing agent	Water	Water
Concentration	0.05 M	± 18.9 M (50 wt%)[a]
pH	± 1.3[b] (at 20 °C)	±14 (at 25 °C)[c]
Electrical conductivity[d]	47.14 mS/cm (at 20 °C)	1293 mS/cm (at 108 °C)

[a] High NaOH concentration can suppress the hydrogen evolution on the cathode side according to [5] and [48].
[b] The pH range of 1.0 – 1.5 provides the optimal trade-off between the undesired hydrogen evolution and the optimum iron deposition in the HCl solutions, according to [12].
[c] pH according to Sigma-Aldrich's safety data sheet.
[d] The electrical conductivity was measured by using a Metrohm 914 pH/conductivity meter, equipped with a Pt1000 temperature sensor/conductivity probe.

solution with Fe_2O_3 powder is mixed by stirring at 300 rpm using a magnetic stirrer for at least 15–20 min. Similar preparation is done for the acidic system, except for the temperature (at room temperature around 20 °C). The mass fraction (ϕ) of hematite powder in the electrolyte mixture is calculated as:

$$\phi = \frac{m_{Fe_2O_3}}{m_{Fe_2O_3} + m_{solvent}} \tag{1}$$

where $m_{Fe_2O_3}$ is the mass of added hematite powder and $m_{solvent}$ is the HCl or NaOH solvent mass. A range of ϕ = 5–20 wt% is investigated in the current study.

2.3.2. Electroreduction process

The electroreduction experiments are conducted at a constant current. Each experiment is performed for one hour, during which the cell voltage (V_{cell}) is recorded. The cathode is weighed before the experiments. After the experiments, it is rinsed gently using demineralized water and then dried for at least about 3 h in a closed petri dish. Afterwards, the cathode with deposits is weighed again to determine the mass of the deposits. Each experiment is repeated at least 3 times to ensure data reproducibility. In this study, current density (j) is described as the ratio of the current (I) and the associated cross-sectional area (A_{front}), which is the cathode surface area facing the anode (15 mm x 40 mm).

2.4. Characterization and analysis

Microstructural characterization of the deposits is carried out using scanning electron microscopy (SEM) (JEOL Ltd., JSM-5600LV, Japan), coupled with elemental analysis by Energy-Dispersive X-Ray Spectroscopy (EDS). The iron purity is quantitatively determined from the weight percentage (wt%) of the iron element.

Reduction performance is primarily evaluated with the Faradaic/current efficiency (η_{cur}), which is defined as the ratio of the real mass of deposits (m_{dep}) and the theoretical Faradic deposit mass (m_{far}):

$$\eta_{cur}(\%) = \frac{m_{dep}}{m_{far}} \times 100 \tag{2}$$

By assuming that all the electrons exchanged are used for the deposition of metallic iron [1,16], the theoretical mass of the deposit follows Faraday's law:

$$m_{far} = \frac{M_{Fe}\, I\, t}{n\, F} \tag{3}$$

where M_{Fe} is the iron molar mass (55.85 g/mol), I is the current supply (A), t is the duration of the experiment (s), and n is the number of electrons involved in the process ($n = 3$ for the transformation of Fe^{3+} to Fe^0). F is the Faraday constant (96,485 C/mol).

The total energy consumption, E_C, (kWh per unit mass of iron deposit) is considered the sum of electrical energy required, E_{el}, and thermal energy, E_{th}, (heating is only for the alkaline system), represented by Eq. (4),

$$E_C = E_{el} + E_{th} \tag{4}$$

with,

$$E_{el} = \frac{V_{cell}\ I\, t}{m_{dep}} \tag{5}$$

and

$$E_{th} = \frac{m_{etl}\ Cp_{etl}\ \Delta T}{m_{dep}\ t} \tag{6}$$

where V_{cell} is the cell voltage, m_{etl} is the electrolyte mass, and ΔT is the difference between system's operating temperature ($110^{\circ}C$) and initial electrolyte temperature ($20^{\circ}C$). In this calculation, all heat losses are neglected and the heat capacity (Cp_{etl}) values of 3.12 kJ/kg.K and 0.65 kJ/(kg·K) are used for the 18.9 M NaOH solution and Fe_2O_3 powder, respectively [28].

3. Results and discussion

3.1. Electrochemical characterization

The electrochemical characteristics of the alkaline and acidic electrolytes are analyzed and compared with chrono-potentiometry and cyclic voltammetry measurements.

3.1.1. Chrono-potentiometry

Chrono-potentiometry measurements, which are carried out by monitoring the cell voltage over time for a constant current, are used to evaluate the required potential to enable the reduction process and the electrochemical stability of both systems. Fig. 5a and b show the chrono-potentiometry results for alkaline and acidic systems, respectively, at blank and Fe_2O_3-addition conditions measured at a constant current supply of 0.4 A.

For the alkaline system (Fig. 5a), the cell voltage of the NaOH electrolyte with Fe_2O_3 addition is slightly lower than that of the blank NaOH solution. This implies a higher conductivity of the Fe_2O_3-addition NaOH electrolyte than the blank electrolyte. This observation is counterintuitive since the added hematite particles are non-conductive. Therefore, it suggests that the solid hematite partially dissolves in the NaOH solution to form iron hydroxide ions [14] that are conductive, which thus lowers the resistance of the electrolyte, as in Eq. (7),

$$\boldsymbol{Fe_2O_3} + 3\ \boldsymbol{H_2O} + 2\ \boldsymbol{OH^-} \rightleftharpoons 2\ \boldsymbol{Fe(OH)_4^-} \quad (7)$$

Furthermore, a cell voltage peak (indicated with the arrow) can be observed for the Fe_2O_3-addition condition. This peak was also observed by Allanore et al. [6] who confirmed the onset of hematite reduction at this point. Moreover, the cell voltages in both alkaline cases quickly reach a steady state. A system with relatively constant cell voltage is preferred in terms of electrical energy consumption.

Conversely, Fig. 5b shows that the cell voltage in the acidic system is much higher when the addition of Fe_2O_3 solids compared to the blank HCl solution. This increase in cell voltage is due to the non-conductive characteristic of the hematite solids that remain as suspended particles in the HCl solution. Furthermore, the presence of the hematite may evolve as an insulating layer [36], which inhibits the local charge transfer between the electrodes and thus further increases cell resistance. Unlike the stable behavior of the alkaline system, the cell voltage in this acidic system does not reach a steady state and keeps increasing over time. This continuous rise of the potential is attributed to the consumption of the charge-carrying ions (H^+) via intense hydrogen evolution reaction, decreasing the electrical conductance. Lastly, the cell voltage in the acidic system is much higher than that in the alkaline system, because of the better electrical conductivity (an order higher) of the NaOH (18.9 M) than the HCl (0.05 M) solution as shown in Table 1.

3.1.2. Cyclic voltammetry (CV)

The cyclic voltammetry curve is obtained by measuring the current at the working electrode while cycling the potential [26]. This CV curve indicates at which potential redox reactions may occur. Fig. 6a and b show the CV curves for alkaline and acidic systems without (blank solution) and with the addition of hematite particles. Both systems have a

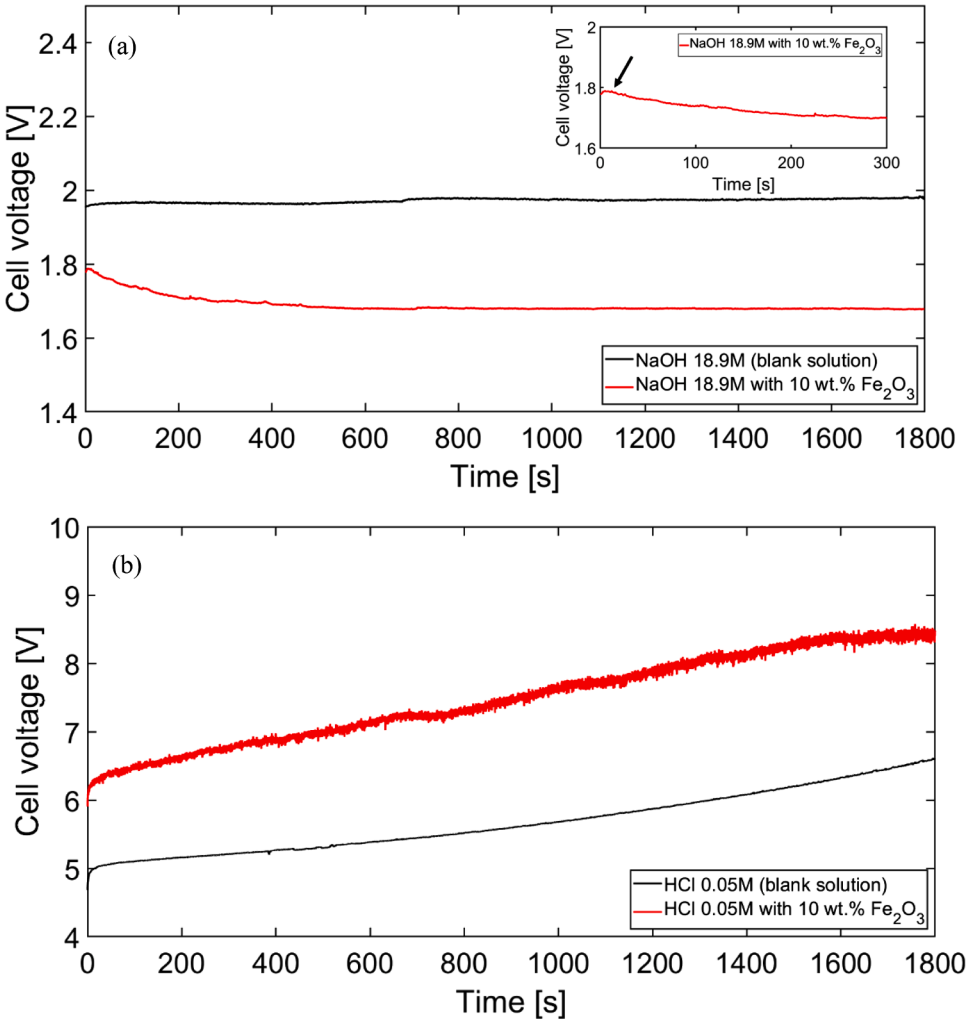

Fig. 5. Examples of chrono-potentiometry curves for (a) an aqueous 18.9 M NaOH solution (T = 110 °C) (b) an aqueous 0.05 M HCl solution (T = 20 °C). Both cases are operated with a constant current of 0.4 A (or j = 666.67 A/m^2). Each figure shows the results of the blank solution (without iron oxide) and a mixture of electrolytes with 10 wt% Fe_2O_3 particles. The cell voltages presented in these curves do not include the ohmic drop. The ohmic drop estimation from the 1-D current flow model is 0.056 V (alkaline system) and 1.565 V (acidic system).

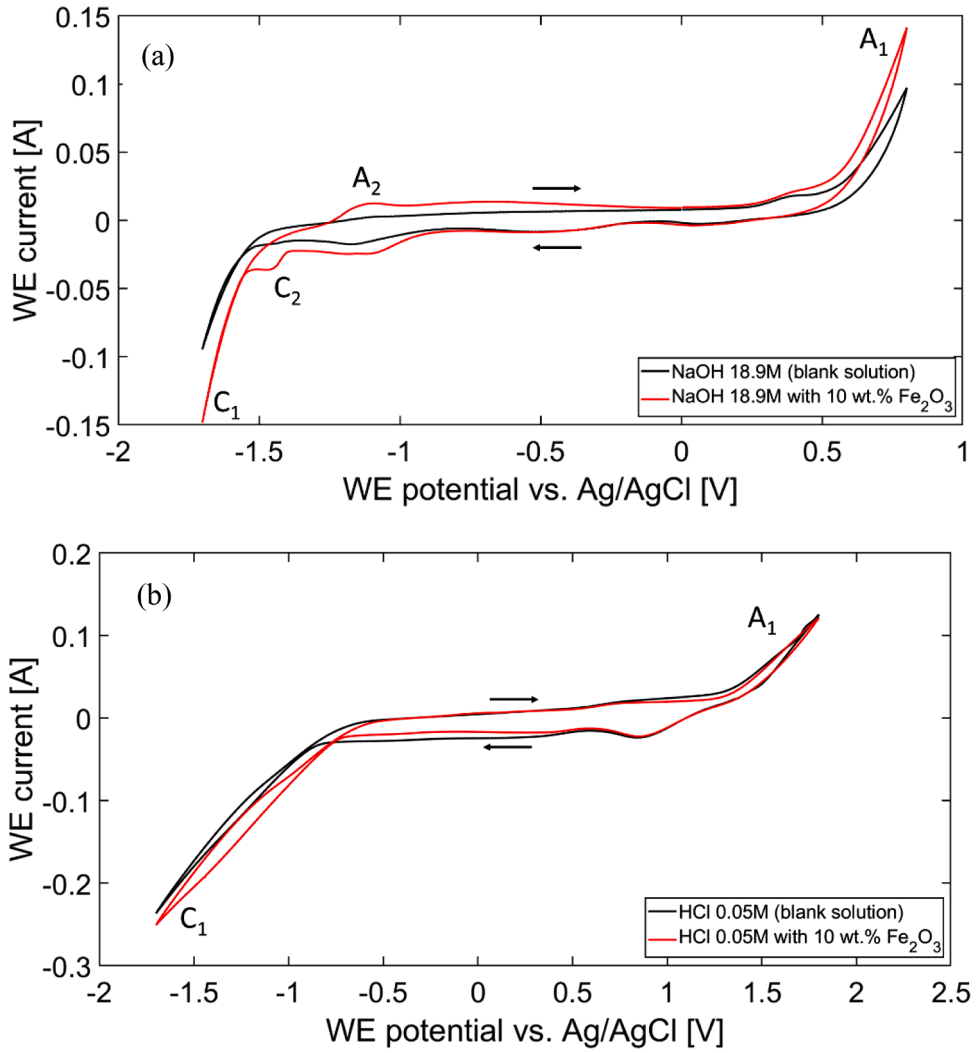

Fig. 6. CV curves of (a) alkaline electrolytes and (b) acidic electrolytes for both a blank solution (without iron oxide) and a mixture with 10 wt% of Fe_2O_3 particles at room temperature (around 20 °C). All curves are taken from the 3rd cycle, with a scan rate of 0.2 V/s. The cathodic peaks (C) indicate the reduction reactions whereas the anodic peaks (A) represent the oxidation reactions. The WE potentials shown in these CVs do not include the ohmic drop.

similar potential window of about 2.0 V (slightly wider in the acidic system).

In the alkaline system shown in Fig. 6a, a sharp cathodic peak C_1 and a sharp anodic peak A_1 are present at both blank and Fe_2O_3-addition conditions. Cathodic peak C_1, starting from approximately –1.53 V (vs. Ag/AgCl), can be assigned to the hydrogen evolution reaction HER (Eq. (8)), whereas the anodic peak A_1, starting from approximately 0.4 V (vs. Ag/AgCl), can be assigned to the oxygen evolution reaction OER (Eq. (9)).

$$\text{HER (at the cathode)} : 2H_2O + 2e^- \rightleftharpoons H_2 + 2OH^- \quad (8)$$

$$\text{OER (at the anode)} : 4\ OH^- \rightarrow O_2 + 2\ H_2O + 4e^- \quad (9)$$

Moreover, the Fe_2O_3-addition system shows additional peaks C_2 and A_2, as compared to the blank condition. This cathodic peak C_2, at a potential of approximately –1.4 V (vs. Ag/AgCl), might indicate the onset of iron reduction. Considering the observation from the chronopotentiometry curves in Fig. 5(a), the multiple reduction steps are suggested, started from the reaction presented in Eq. (7) and followed by the reduction of $Fe(OH)^{4-}$ to $Fe(OH)^{3-}$ in solution as shown in Eq. (10). Finally, a complete reduction reaction as shown in Eq. (11) and cathodic deposition of metallic iron occurs. This mechanism aligns with studies from Le and Ghali [29], Beverskog and Puidgomenech [10], and Allanore et al. [2]. In addition, we suggest that the abovementioned mechanism occurs simultaneously with Fe_2O_3 particle adsorption (due to electrostatic force) onto the cathode's surface [4], as also stated by Lopes et al. [34]. However, further studies are still needed to confirm a better understanding of the mechanism.

$$Fe(OH)_4^- + e^- \rightarrow Fe(OH)_3^- + OH^- \quad (10)$$

$$Fe(OH)_3^- + 2e^- \rightarrow Fe + 3\ OH^- \quad (11)$$

Lastly, the anodic peak A_2, at a potential of approximately –1.1 V (vs. Ag/AgCl), might suggest reverse reactions of iron reduction, namely the conversion of metallic iron to iron hydroxide followed by even further oxidation to magnetite [2,31], as shown in Eqs. (12 and 13).

$$Fe + 2\ OH^- \rightarrow Fe(OH)_2 + 2\ e^- \quad (12)$$

$$3\ Fe(OH)_2 + 2OH^- \rightarrow Fe_3O_4 + 4\ H_2O + 2e^- \quad (13)$$

In the acidic system Fig. 6b), both CV curves at the blank and Fe_2O_3-addition conditions resemble each other. The sharp peaks at 1.4 V (vs Ag/AgCl) and –0.3 V (vs Ag/AgCl), similar to A_1 and C_1 in alkaline systems, represent the oxygen and hydrogen evolution reactions, as shown in Eqs. (8 and (9).

The difference in CV behavior between alkaline and acidic

electrolytes shown in Fig. 6 are in good agreement with the potential-pH relationship indicated in the Pourbaix diagram (Fig. 1). The potentials for the HER and OER decrease with increasing pH. This explains the shifting of the alkaline system's CV curves to the lower potentials as compared to those of the acidic system. However, the Pourbaix diagram implies that iron oxide reduction is possible in both alkaline and acidic electrolytes, whereas no obvious sign is shown from the CV curves of the acidic system.

3.2. Morphology of the deposit

Morphology and microstructure of the deposit after the electroreduction process in alkaline and acidic systems are shown in Fig. 7. For the alkaline system, the residual electrolyte-hematite mixture can be easily cleaned off the cathode by just rinsing with water, resulting in black colored deposit surface. However, in the acidic system, the residual hematite particles/layer attached to the cathode cannot be easily rinsed off, thus we see reddish color at the surface of the deposition. These phenomena differences can be explained by particle surface charge in different solutions. Hematite particles are slightly positively charged in acidic solutions and slightly negatively charged in alkaline solutions [43]. Positively charged iron oxide particles in the acidic electrolyte may be attracted by the negatively charged cathode. Therefore, the charged iron oxides would strongly stick, making the rinsing/cleaning very challenging. Note that these hematite residuals remain only at the surface. As shown in Fig. 8a, underneath this reddish hematite layer the metallic iron (black layer) is present. As a result, this introduces challenges/errors in the determination of deposit mass and the purity of iron deposition, as shown in the EDS result (Fig. 8c). Overall, for both systems, uniform and compact iron deposits are observed at the front-face area while brittle dendritic structures are present at the corners and edges of the cathode. As for the purity of the deposits, above 98 wt% of metallic iron is identified from the deposits in the alkaline system. For the acidic system, we believe in the potential of high iron purity, however, we cannot directly measure because of the hematite residual layer as described above.

Fig. 7 also indicates that the microstructures of the dendritic iron deposition are totally different from these two systems. The SEM images of dendrites which are obtained from the alkaline system reveal that the deposit consists of crystalline and hexagonal pyramid-like microstructures. Tetrahedral configurations in the deposit crystals converge towards the vertex tip. These structures grow continuously at varying angles starting from the cathode surface in a perpendicular direction. Close to the electrode surface (baseline), crystals are smaller while larger crystals are grown further from the cathode. The observed microstructure for iron deposit in alkaline system has a high similarity to what has been reported by the previous studies with alkaline system in various configuration systems such as rotating disc electrode/RDE [48] and parallel plate system with a flowing electrolyte flow [5]. Different from the alkaline system, the SEM images of dendrites resulted from the acidic system show porous deposit with micro-dendritic structures. These two different microstructure types might indicate different electrodeposition mechanisms, which require further investigation. One possible explanation might be due to the higher hydrogen evolution in the acidic system, which results in massive bubbles contributing to the brittleness and porous microstructure of the deposits [17,23].

3.3. Electroreduction performance

3.3.1. Current efficiency

Fig. 9 compares the current efficiency (defined in Section 2.4) of iron deposition in alkaline and acidic systems at different hematite mass fractions and two different current densities. Overall, the current efficiency achieved in the alkaline system is relatively high and stabilizes at

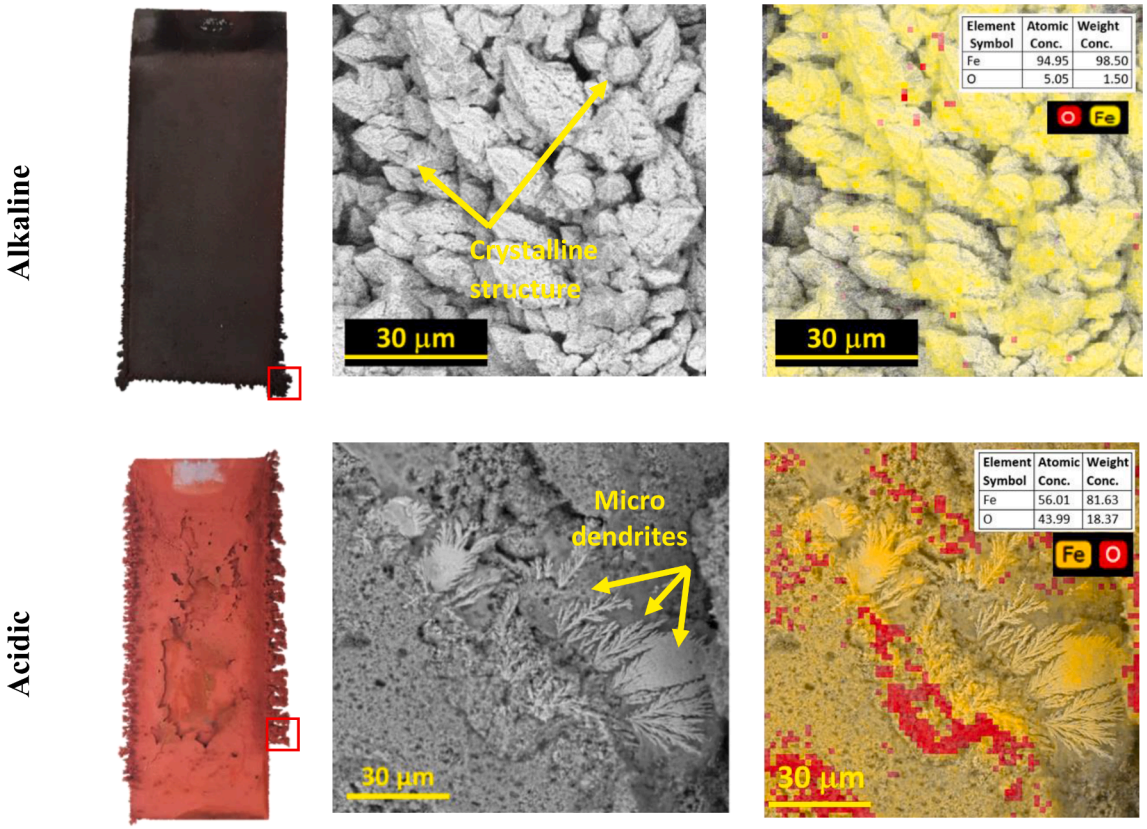

Fig. 7. Cathode with deposition after rinsing and drying processes (left), SEM images of the deposit corresponding to the selected area (red square) after electroreduction in alkaline and acidic media (middle), and results of EDS mapping (right). The experiment conditions are: $j = 2000$ A/m^2 and $\phi = 10$ wt%.

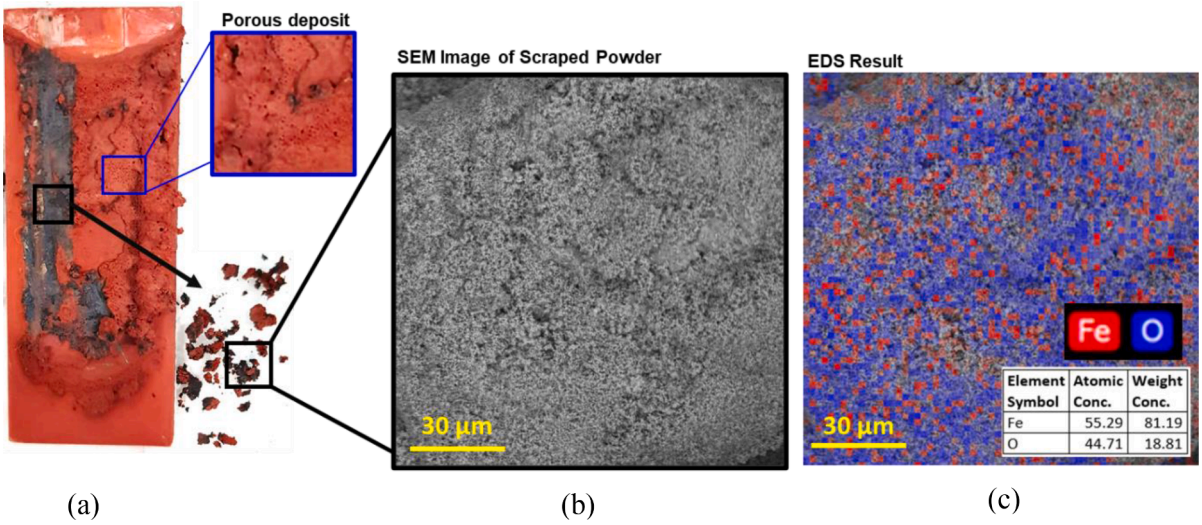

Fig. 8. (a) Preview of the scraped electrode after the acidic experiment followed by SEM image (b) and the result of EDS mapping (c) of powder taken from the selected scraped area (black box). The picture in the blue box (of Fig. 8a) is the magnification of porous deposit on the surface. The experiment conditions are: j = 2000 A/m^2 and ϕ = 10 wt%.

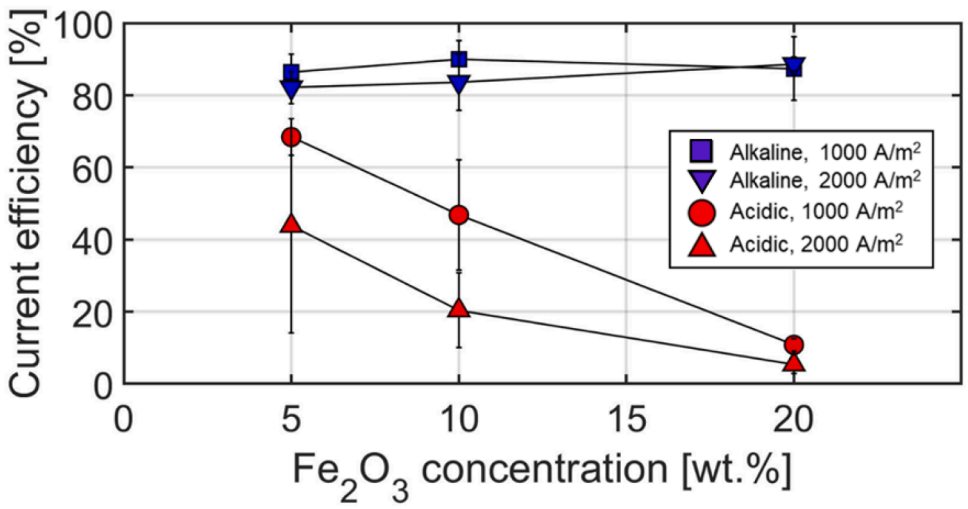

Fig. 9. Current efficiency as a function of Fe_2O_3 mass fraction for the acidic and alkaline electrolyte with current densities of 1000 A/m^2 and 2000 A/m^2, after 1-hour experiments. Real values for the acidic electrolyte are likely to be lower due to the hematite residual layer contributing to the weighted mass, as explained in Section 3.2.

above 80%−90% for all the tested conditions of hematite mass concentration and current density. This result is slightly contradictory to some literature (e.g. Ahamed et al., [1] – for the small current densities of 206−1000 A/m^2) where the current efficiency is reported to increase with increasing current density; but these results are in line with LeDuc et al. [30]. As for the effect of hematite concentration, a mass concentration of about 10% can be determined optimal from our experiments. This has mainly resulted from the combined effects of solid concentration on solubility and electrical conductivity of the electrolyte.

The current efficiency in the acidic system is overall lower than in the alkaline system and is found to decrease with increasing solid concentration and current density. As discussed in Section 3.1, the hydrogen evolution reaction is unavoidable and much more severe in the acidic system. The change in equilibrium potential of the H_2 or H^+ with pH can aggravate the competition with the desired metal formation (metallic iron), particularly in the acidic system. Subsequently, when current density/current supply increases, it triggers the pronounced HER which is a competing reaction to the iron reduction. Furthermore, when the solids concentration increases, the electrical conductivity of the acidic electrolyte mixture decreases as shown by the increased cell potential in Fig. 6b. In addition, the attraction of positively charged hematite particles to the negatively charged cathode might lead to an insulation layer which inhibits effective electron transfer between anode to cathode. Increasing solid concentration enhances the formation of this insulation layer. All these reasons contribute to the decrease in current efficiency.

3.3.2. *Energy consumption*

Fig. 10 shows the total energy consumption (per unit mass of iron deposition) of the best cases (the lowest energy consumption per unit mass of deposit) of alkaline (j = 4000 A/m^2, ϕ = 20 wt%, η_{cur} = 88.8%) and acidic (j = 1000 A/m^2, ϕ = 5 wt%, η_{cur} = 64.8%) systems. The thermal energy, required for the elevated temperature of 110 °C during the experiment duration (1 h) contributes to roughly 2/3 of the total energy cost in the alkaline system. Comparing these two systems, we see that even with extra thermal energy, the total energy consumption in the alkaline system is still much lower than that in the acidic system. This is basically a consequence of the lower current efficiency (less iron deposit mass) in the acidic system as shown in Fig. 9. If future studies can

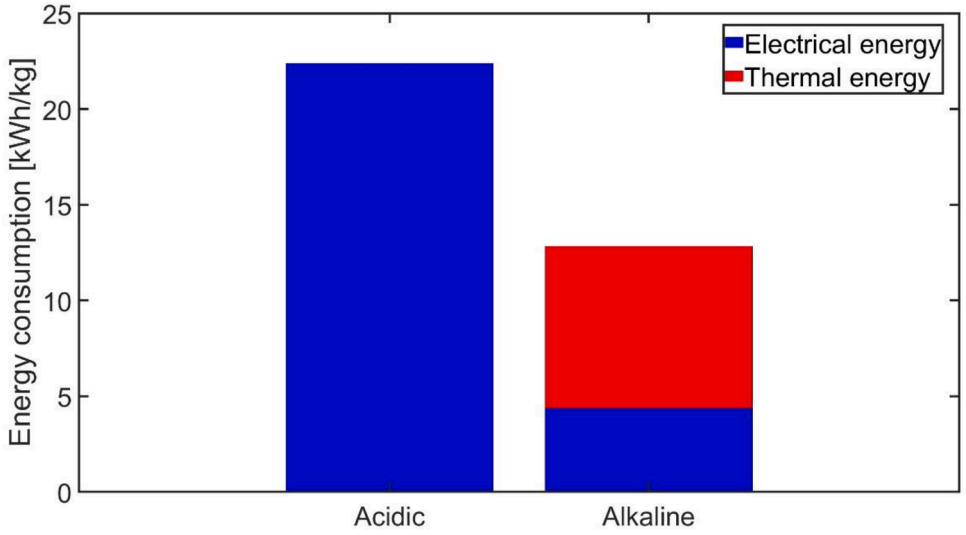

Fig. 10. Total energy consumption for acidic and alkaline electrolytes with the highest current efficiencies (best cases): alkaline system ($j = 4000$ A/m^2 and $\phi = 20$ wt%) and acidic system ($j = 1000$ A/m^2 and $\phi = 5$ wt%).

improve the current efficiency in acidic systems, it might become a competitive advantage to the alkaline route in terms of energy consumption/efficiency. In these two particular cases, the acidic electrolyte consumes a total energy of 22.44 kWh/kg of iron deposition, while the alkaline system requires 12.83 kWh/kg of iron deposition (with E_{el} of 4.38 kWh/kg of iron deposition).

4. Conclusions

The characteristics and performance of electroreduction of iron oxide in alkaline and acidic electrolytes are analyzed and compared through theoretical and experimental studies. The results indicate that although the iron electrodeposition from iron oxides is theoretically feasible in both acidic and alkaline systems, the practical realization is much more difficult under acidic conditions due to much more pronounced hydrogen evolution. At strong alkaline conditions, the HER can be mostly suppressed, leading to higher current efficiency of iron deposition. From our experiments, a stable current efficiency of above 90% has been achieved in the alkaline system. As far as energy efficiency is concerned, the consumption per unit mass iron deposition is much higher for the acidic system (due to lower current efficiency) than for the alkaline system despite that additional thermal energy is required to heat up the alkaline system (e.g. at 110 °C).

In both systems, high-purity metallic iron deposits are obtained. However, in the acidic system, the hematite particles adhesion to the surface of the cathode due to the opposite charges, which are difficult to rinse off thus hindering the harvest of the deposited metallic iron. Furthermore, the form of the deposit and its microstructure obtained in these two systems differ significantly from each other. The metallic iron dendrites in the alkaline system show crystalline microstructures, while the deposits in the acidic system consist of heterogeneous porous layers with fine dendritic microstructure.

In all, the alkaline system shows more attractive results and better feasibility for the application of low-temperature iron oxide electroreduction in the context of "*powder to powder*" as for the application of iron fuel. This study provides useful insights into the field of iron oxide electroreduction, which is applicable to enable sustainable iron/steel production and recyclable iron fuel realization. Future works should focus on improving the efficiency of the process, particularly in the control of the reactions at the cathode where the desired reduction reaction is competing with the evolution of hydrogen gas, especially for the acidic medium. Furthermore, some attempts related to thermal management (i.e., the use of lower temperatures and heat recovery) can potentially increase the energy efficiency of electroreduction in alkaline systems.

Research Funding

Financial support was provided by Ministry of Education, Culture, Research, and Technology of the Republic of Indonesia.

CRediT authorship contribution statement

Akmal Irfan Majid: Conceptualization, Methodology, Investigation, Data curation, Formal analysis, Writing – original draft, Writing – review & editing, Funding acquisition. **Niels van Graefschepe:** Methodology, Investigation, Data curation, Formal analysis, Writing – original draft. **Giulia Finotello:** Conceptualization, Supervision, Writing – review & editing, Funding acquisition. **John van der Schaaf:** Conceptualization, Resources, Supervision. **Niels G. Deen:** Conceptualization, Methodology, Supervision, Project administration, Funding acquisition. **Yali Tang:** Conceptualization, Methodology, Supervision, Writing – review & editing, Project administration, Funding acquisition.

Declaration of Competing Interest

The authors declare the following financial interests/personal relationships which may be considered as potential competing interests:

Akmal Irfan Majid reports financial support is provided by Ministry of Education, Culture, Research, and Technology of the Republic of Indonesia.

Data availability

Data will be made available on request.

Acknowledgements

Akmal Irfan Majid acknowledges a scholarship for the doctoral program from the Ministry of Education, Culture, Research, and Technology of the Republic of Indonesia through a "BPP-LN" scholarship scheme, contract number: B/823/D3.2/KD.02.01/2019. The authors sincerely thank people from the SPE Group of Chemical Engineering and Chemistry (CEC) of TU Eindhoven, among them are Rodrigo Lira Garcia Barros, PD. Eng., Dr. M.T. (Thijs) de Groot, and Dr. Amin Delparish for

valuable technical discussions, also Ing. Carlo Buijs and Ing. Peter Lipman for their technical support during the experimental works. We are also indebted to Niek van Rooij from Metalot for helping us with particle size measurement.

References

[1] A.M. Ahamed, M.N. Pons, Q. Ricoux, F. Goettmann, F. Lapicque, Production of electrolytic iron from red mud in alkaline media, J. Environ. Manage. 266 (2020), 110547, https://doi.org/10.1016/j.jenvman.2020.110547.

[2] A. Allanore, H. Lavelaine, G. Valentin, J.P. Birat, F. Lapicque, Electrodeposition of metal iron from dissolved species in alkaline media, J. Electrochem. Soc. 154 (12) (2007) E187, https://doi.org/10.1149/1.2790285.

[3] A. Allanore, H. Lavelaine, G. Valentin, J.P. Birat, F. Lapicque, Iron metal production by bulk electrolysis of iron ore particle in aqueous media, J. Electrochem. Soc. 155 (9) (2008) E125–E129, https://doi.org/10.1149/1.2952547.

[4] A. Allanore, H. Lavelaine, G. Valentin, J.P. Birat, P. Delcroix, F. Lapicque, Observation and modeling of the reduction of hematite particles to metal in alkaline solution by electrolysis, Electrochim. Acta 55 (12) (2010) 4007–4013, https://doi.org/10.1016/j.electacta.2010.02.040.

[5] A. Allanore, H. Lavelaine, J.P. Birat, G. Valentin, F. Lapicque, Experimental investigation of cell design for the electrolysis of iron oxide suspensions in alkaline electrolyte, J. Appl. Electrochem. 40 (2010) 1957–1966, https://doi.org/10.1007/s10800-010-0172-0.

[6] A. Allanore, J. Feng, H. Lavelaine, K. Ogle, The adsorption of hematite particles on steel in strongly alkaline electrolyte, J. Electrochem. Soc. 157 (3) (2010) E24, https://doi.org/10.1149/1.3273198.

[7] A. Allanore, Features and challenges of molten oxide electrolytes for metal extraction, J. Electrochem. Soc. 162 (1) (2015) E13–E22, https://doi.org/10.1149/2.0451501jes.

[8] M. Bailera, P. Lisbona, B. Peña, L.M. Romeo, A review on CO_2 mitigation in the iron and steel industry through power to X processes, J. CO_2 Util. 46 (2021), https://doi.org/10.1016/j.jcou.2021.101456.

[9] J.M. Bergthorson, Recyclable metal fuels for clean and compact zero-carbon power, Prog. Energy Combust. Sci. 68 (2018) 169–196, https://doi.org/10.1016/j.pecs.2018.05.001.

[10] B. Beverskog, I. Puigdomenech, Revised Pourbaix diagrams for ion at 25-300 °C, Corros. Sci. 38 (1996) 2121–2135, https://doi.org/10.1016/S0010-938X(96)00067-4.

[11] R.M. Cornell, U. Schwertmann, The Iron Oxides: Structure, Properties, Reactions, Occurrences and Uses, 2nd Edition, Wiley-VCH, Weinheim, 1996.

[12] G. Csicsovszki, T. Kékesi, T.I. Török, Selective recovery of Zn and Fe from spent pickling solutions by the combination of anion exchange and membrane electrowinning techniques, Hydrometallurgy 77 (1–2) (2005) 19–28, https://doi.org/10.1016/j.hydromet.2004.10.020.

[13] P. Debiagi, R.C. Rocha, A. Scholtissek, J. Janicka, C. Hasse, Iron as a sustainable chemical carrier of renewable energy: analysis of opportunities and challenges for retrofitting coal-fired power plants, Renew. Sustain. Energy Rev. 165 (2022), 112579, https://doi.org/10.1016/j.rser.2022.112579.

[14] I.I. Diakonov, J. Schott, F. Martin, J.C. Harrichourry, J. Escalier, Iron(III) solubility and speciation in aqueous solutions. Experimental study and modelling: part 1. Hematite solubility from 60 to 300 °C in NaOH-NaCl solutions and thermodynamic properties of $Fe(OH)_{4(aq)}^-$, Geochim. Cosmochim. Acta 63 (1999) 2247–2261, https://doi.org/10.1016/S0016-7037(99)00070-8.

[15] S.L. Díaz, J.A. Calderón, O.E. Barcia, O.R. Mattos, Electrodeposition of iron in sulphate solutions, Electrochim. Acta 53 (25) (2008) 7426–7435, https://doi.org/10.1016/j.electacta.2008.01.015.

[16] V. Feynerol, H. Lavelaine, P. Marlier, M.N. Pons, F. Lapicque, Reactivity of suspended iron oxide particles in low temperature alkaline electrolysis, J. Appl. Electrochem. 47 (12) (2017) 1339–1350, https://doi.org/10.1007/s10800-017-1127-5.

[17] D.R. Gabe, The role of hydrogen in metal electrodeposition processes, J. Appl. Electrochem. 27 (1997) 908–915, https://doi.org/10.1023/A:1018497401365.

[18] K.M. Gorbunova, L.I. Liamina, On the mechanism of iron reduction from alkaline solutions, Electrochim. Acta 11 (5) (1966) 457–467, https://doi.org/10.1016/0013-4686(66)80023-3.

[19] G.M. Haarberg, B. Qin, B. Khalaghi, Electrochemical reduction of iron oxides in aqueous NaOH electrolyte including iron residue from nickel and zinc electrowinning processes, *Miner., Metals Mater. Series, Part F* (2022) 341–347, https://doi.org/10.1007/978-3-030-92662-5_33.

[20] IEA. (2022). Iron and steel, *https://www.iea.org/reports/iron-and-steel*.

[21] K. Ishikawa, T. Yoshioka, T. Sato, A. Okuwaki, Solubility of hematite in LiOH, NaOH, and KOH solutions, Hydrometallurgy 45 (1–2) (1997) 129–135, https://doi.org/10.1016/S0304-386X(96)00068-0.

[22] Y.A. Ivanova, J.F. Monteiro, L.B. Teixeira, N. Vitorino, A.V. Kovalevsky, J.R. Frade, Designed porous microstructures for electrochemical reduction of bulk hematite ceramics, Mater. Des. 122 (2017) 307–314, https://doi.org/10.1016/j.matdes.2017.03.031.

[23] M. Izaki, Electrodeposition of iron and iron alloys, in: M. Schlesinger, M. Paunovic (Eds.), Mod. Electroplat, 5th edition, John Wiley Sons, Inc., 2010, pp. 309–326, https://doi.org/10.1007/BF01022244.

[24] P. Julien, J.M. Bergthorson, Enabling the metal fuel economy: green recycling of metal fuels, Sustain. Energy Fuels 1 (3) (2017) 615–625, https://doi.org/10.1039/c7se00004a.

[25] J. Kim, B.K. Sovacool, M. Bazilian, S. Griffiths, J. Lee, M. Yang, J. Lee, Decarbonizing the iron and steel industry: a systematic review of sociotechnical systems, technological innovations, and policy options, Energy Res. Soc. Sci. 89 (February) (2022), 102565, https://doi.org/10.1016/j.erss.2022.102565.

[26] P.T. Kissinger, W.R. Heineman, Cyclic voltammetry, J. Chem. Educ. 60 (702) (1983), https://doi.org/10.1021/ed060p702.

[27] S. Koutsoupa, S. Koutalidi, E. Balomenos, D. Panias, ΣIDERWIN—a new route for iron production, Mater. Proc. 5 (1) (2021) 58, https://doi.org/10.3390/materproc2021005058.

[28] M. Laliberté, A model for calculating the heat capacity of aqueous solutions, with updated density and viscosity data, J. Chem. Eng. Data 54 (6) (2009) 1725–1760, https://doi.org/10.1021/je8008123.

[29] H. Le, E. Ghali, Interpretation des diagrammes E-pH du systeme FeH_2O en relation avec la fragilisation caustique des aciers, J. Appl. Electrochem. 23 (1993) 72–77, https://doi.org/10.1007/BF00241579.

[30] J.A.M. LeDuc, R.E. Loftfield, L.E. Vaaler, Electrolytic iron powder from a caustic soda solution, J. Electrochem. Soc. 106 (1) (1952) 659–667, https://doi.org/10.1149/1.2427467.

[31] D.V. Lopes, A. Kovalevsky, M. Quina, J. Frade, Electrochemical deposition of zero-valent iron from alkaline ceramic suspensions of $Fe_{2-x}Al_xO_3$ for iron valorisation, J. Electrochem. Soc. 167 (10) (2020), 102508, https://doi.org/10.1149/1945-7111/ab9a2b.

[32] D.V. Lopes, A.D. Lisenkov, S.A. Sergiienko, G. Constantinescu, A. Sarabando, M. J. Quina, J.R. Frade, A.V. Kovalevsky, Alkaline electrochemical reduction of a magnesium ferrospinel into metallic iron for the valorisation of magnetite-based metallurgical waste, J. Electrochem. Soc. 168 (7) (2021), 073504, https://doi.org/10.1149/1945-7111/ac1490.

[33] Z.Y. Lu, D.M. Muir, Dissolution of metal ferrites and iron oxides by HCl under oxidising and reducing conditions, Hydrometallurgy 21 (1) (1988) 9–21, https://doi.org/10.1016/0304-386X(88)90013-8.

[34] D.V. Lopes, M.J. Quina, J.R. Frade, A.V. Kovalevsky, Prospects and challenges of the electrochemical reduction of iron oxides in alkaline media for steel production, Front. Mater. 9 (2022), 1010156, https://doi.org/10.3389/fmats.2022.1010156.

[35] J.F. Monteiro, Y.A. Ivanova, A.V. Kovalevsky, D.K. Ivanou, J.R. Frade, Reduction of magnetite to metallic iron in strong alkaline medium, Electrochim. Acta 193 (2016) 284–292, https://doi.org/10.1016/j.electacta.2016.02.058.

[36] F.J. Morin, Electrical properties of αFe_2O_3, and αFe_2O_3 containing titanium, Phys. Rev. 83 (5) (1951) 1005–1011, https://doi.org/10.1103/PhysRev.83.1005.

[37] E. Mostad, S. Rolseth, J. Thonstad, Electrowinning of iron from sulphate solutions, Hydrometallurgy 90 (2–4) (2008) 213–220, https://doi.org/10.1016/j.hydromet.2007.07.014.

[38] J. Ning, Y.G. Zheng, B. Brown, D.J. Young, S. Nešić, Construction and verification of pourbaix diagrams for hydrogen sulfide corrosion of mild steel, in: Corrosion 2015 Conference and Expo, 2015, p. 5507. Paper number.

[39] K.M. Parida, N.N. Das, Reductive dissolution of hematite in hydrochloric acid medium by some inorganic and organic reductants: a comparative study, In *Indian J. Eng. Mater. Sci.* 3 (1996) 243–247.

[40] S. Pauliuk, R.L. Milford, D.B. Müller, J.M. Allwood, The steel scrap age, Environ. Sci. Technol. 47 (7) (2013) 3448–3454, https://doi.org/10.1021/es303149z.

[41] M. Pourbaix, Atlas of Electrochemical Equilibria In-Aqueous Solutions, 2nd Edition, USA: National Association of Corrosion Engineers and Brussels, Cebelcor, 1974.

[42] M.A. Quader, S. Ahmed, R.A.R. Ghazilla, S. Ahmed, M. Dahari, A comprehensive review on energy efficient CO_2 breakthrough technologies for sustainable green iron and steel manufacturing, Renew. Sustain. Energy Rev. 50 (2015) 594–614, https://doi.org/10.1016/j.rser.2015.05.026.

[43] G. Toikka, R.A. Hayes, J. Ralston, Adhesion of iron oxide to silica studied by atomic force microscopy, J. Colloid Interface Sci. 180 (2) (1996) 329–338, https://doi.org/10.1006/jcis.1996.0311.

[44] M. Tokushige, O.E. Kongstein, G.M. Haarberg, Crystal orientation of iron produced by electrodeoxidation of hematite particles, ECS Trans. 50 (52) (2013) 103–114, https://doi.org/10.1149/05052.0103ecst.

[45] P. Vehmaanperä, R. Salmimies, A. Häkkinen, Thermodynamic and kinetic studies of dissolution of hematite in mixtures of oxalic and sulfuric acid, Mining, Metall. Explor. 38 (1) (2021) 69–80, https://doi.org/10.1007/s42461-020-00308-4.

[46] J. Wiencke, H. Lavelaine, P.J. Panteix, C. Petitjean, C. Rapin, Electrolysis of iron in a molten oxide electrolyte, J. Appl. Electrochem. 48 (1) (2018) 115–126, https://doi.org/10.1007/s10800-017-1143-5.

[47] WSA. World steel in figures 2022, *https://worldsteel.org/steel-topics/statistics/world-steel-in-figures-2022*.

[48] B. Yuan, O.E. Kongstein, G.M. Haarberg, Electrowinning of iron in aqueous alkaline solution using a rotating cathode, J. Electrochem. Soc. 156 (2) (2009) D64, https://doi.org/10.1149/1.3039998.

[49] X. Zhang, K. Jiao, J. Zhang, Z. Guo, A review on low carbon emissions projects of steel industry in the world, J. Clean. Prod. 306 (2021), 127259, https://doi.org/10.1016/j.jclepro.2021.127259.

[50] X. Zou, S. Gu, X. Lu, X. Xie, C. Lu, Z. Zhou, W. Ding, Electroreduction of iron(III) oxide pellets to iron in alkaline media: a typical shrinking-core reaction process, Metall. Mater. Trans. B: Process Metall. Mate. Process. Sci. 46 (3) (2015) 1262–1274, https://doi.org/10.1007/s11663-015-0336-8.